Fluctuations from cosmic strings and the microwave background

Robert H. Brandenberger* and Neil Turok†
Institute for Theoretical Physics, University of California, Santa Barbara, California 93106
(Received 30 July 1985)

The spectrum of energy-density perturbations and anisotropies in the microwave background radiation are calculated in models with cosmic strings. The computations are based on a mathematical model of the network of cosmic strings as a combination of a random walk of infinite strings and a distribution of string loops. The energy-density distribution is scale invariant at Hubble radius crossing, but the k dependence of the spectrum is nontrivial and not equal to the result for adiabatic linear perturbations. The anisotropies in the microwave background radiation are smaller than the observational upper bounds on all angular scales for a value $\mu G \sim 2\times 10^{-6}$ obtained from independent astrophysical considerations. We include both the effects due to gravitational lensing from long strings and from local gravitational perturbations due to loops (the Sachs-Wolfe effect).

I. INTRODUCTION

Cosmic strings have recently generated considerable interest as a mechanism for forming structures in the Universe such as galaxies and clusters of galaxies. In the usual picture, structures are formed by the collapse of initially linear adiabatic energy-density perturbations arising, for example, as a consequence of quantum fluctuations in the de Sitter phase of an inflationary universe. According to the present numerical simulations (see, e.g., Ref. 1 for a recent review) no candidate for dark matter with these perturbations can satisfy in a natural way all the cosmological constraints.

Cosmic strings are one-dimensional topological defects which are formed in certain grand unified theories during a phase transition in the early Universe. Zel'dovich[2] and Vilenkin,[3] based on earlier work by Kibble,[4] first realized that energy-density perturbations generated by these strings have the right order of magnitude to allow for the formation of galaxies and clusters. See Ref. 5 for recent reviews.

In this paper we develop a mathematical model to describe a network of cosmic strings. Using parameters recently determined in numerical simulations,[6,7] we are able to determine in a more precise manner than hitherto[8-10] the detailed cosmological consequences of cosmic strings. In particular, we compute the energy-density correlation function, discuss a model of accretion of matter around string loops, and take a first look at the fluctuations in the microwave background radiation induced in these models.

The cosmic string theory of galaxy formation has only one free parameter: the mass per unit length μ. In a previous paper[11] we determined μ from astrophysical considerations. Here we conclude that given this value of μ the predicted anisotropies in the microwave background radiation are smaller than the best current observational limits. The spectrum of energy-density perturbations is scale invariant at Hubble radius crossing, but does not have the usual wave-number dependence from linear perturbation theory.

The outline of this paper is as follows. In Sec. II we summarize known results concerning the formation and evolution of a network of cosmic strings. We describe the analytical model of the network of strings on which the subsequent calculations are based. In Sec. III we discuss the spectrum of energy-density fluctuations before recombination. Accretion of baryons around strings begins after recombination. In Sec. IV we discuss the spherical collapse model which models accretion and compute the resulting energy density fluctuations. Next, we take a first look at the effects on the cosmic microwave background radiation. We discuss anisotropies due to the gravitational field of long strings and present a Newtonian analysis of the Sachs-Wolfe effect,[12] the distortions in the microwave background due to local energy density perturbations along the light rays. In Sec. VI we summarize the main results.

We will be working in the context of a Friedmann-Robertson-Walker cosmology with scale factor $a(t)$.

We will consider both hot and cold dark matter. The main difference between the two scenarios is the time when accretion begins. Hot dark matter is relativistic before recombination and will not cluster. Accretion can start only after recombination. Cold dark matter on the other hand will start to cluster immediately after the time t_{eq} of equal matter and radiation. At decoupling t_{dec} baryons will fall into the regions of overdensity set up by the cold dark matter. The calculations in Secs. III and IV will be performed assuming no cold dark matter. At the end of each section we will comment on the changes in cold-dark-matter scenarios.

II. FORMATION AND EVOLUTION OF COSMIC STRINGS

Cosmic strings of the type we shall discuss here are predicted by a large range of grand unified theories and in particular those based on superstring theories. The requirement for strings to be formed is that as the Universe cools and a Higgs field Φ acquires a nonvanishing vacuum expectation value, the manifold of degenerate vacua

M_0 of the Higgs field in question is nonsimply connected. This makes it possible that as one traverses a loop in space $\mathbf{x}(\sigma)$, $\Phi(\mathbf{x}(\sigma))$ will traverse a noncontractible loop in M_0. If one then imagines contracting the loop $\mathbf{x}(\sigma)$ to a point, $\Phi(\mathbf{x}(\sigma))$ must leave M_0, giving a localized distribution of energy density. Since the loop in configuration space is incontractible it follows that the energy density distribution can have no ends [since otherwise one could contract $\mathbf{x}(\sigma)$ around one end]. The localized distributions of energy density, the strings, are either infinite or in the form of closed strings. Their width is determined by a balance between gradient and potential energy.

The manner in which the field Φ arrives at such a configuration depends on the details of the phase transition. As noted by Kibble[4] if the transition occurs sufficiently rapidly, the field Φ is quenched and on scales larger than some coherence length L simply chooses to fall at random to values in M_0. Now, as one traverses loops in space with radii larger than L, Φ sometimes traverses a noncontractible path in M_0 and strings are formed.

L determines the density of strings at formation, $\rho_s \sim \mu/L^2$, where μ is the mass per unit length of the string. The value of L depends on the coupling constants of the theory considered. If the phase transition is noninflationary, $L < 2t$, the horizon size, giving $\rho_s > \mu/4t^2$ at formation.

Numerical simulations of the process of formation of strings[6,13] have shown that about 80% of the resulting string density is in the form of infinite open lengths with the fractal dimension of a Brownian walk,[14] while the rest is in the form of closed loops.

As the Universe expands, the network of infinite strings is stretched[15] and straightened out. The coherence length L grows with t. Strings intersect frequently. There is a probability p that strings which cross will exchange partners and reconnect the other way. If $p=0$ then the energy in strings scales as matter in a radiation-dominated background.[15,16] This would be a cosmological disaster, since strings would come to dominate the energy density of the Universe. If $p \simeq 1$ the number of infinite strings per comoving volume will decrease as the strings chop themselves up into loops with radii of order the horizon size. Numerical simulations[6] have shown that in this case the energy density in strings decreases as radiation. The same conclusion was obtained analytically[16] under the assumption that the system is characterized by a single scale.

Loops of strings smaller than the horizon retain constant physical size. They oscillate with a period equal to one-half their length and lose energy at a constant rate due to gravitational radiation until they disappear.[3,17] At any given time t there are loops which were formed between t and $\gamma\mu G t$. γ is a constant of order unity which can be determined from numerical analyzes and calculations of gravitational radiation.[17,18] These yield $\gamma \simeq 5$.

The above analytical and numerical results justify the following model of the network of cosmic strings. The network consists of a set of infinite strings and a distribution of finite-size string loops. We model the set of infinite strings as a random walk with step length

$$L(t) = \lambda t \ . \tag{1}$$

λ is a constant of order unity. According to numerical simulations,[6,7] $\lambda \simeq 2$. The total energy density in infinite strings, ρ_s, is scale invariant:

$$\rho_s = \alpha\mu L^{-2} \ . \tag{2}$$

Here $\alpha \sim 8$.

The distribution of loops is characterized by the number density $n(R)dR$ of loops of radius between R and $R+dR$. $n(R)$ is proportional to R^{-4} at Hubble radius crossing as a consequence of scale invariance.[3,16,17] Inside the Hubble radius, the number density red-shifts. Hence in the radiation-dominated period

$$n(R) = \nu R^{-4} \left[\frac{r}{t} \right]^{3/2} = \nu R^{-5/2} t^{-3/2} \ . \tag{3}$$

ν is a constant determined from numerical simulations: $\nu \simeq 0.01$. After the time $t_{\rm eq}$ of equal matter and radiation

$$n(R) = \nu R^{-5/2} t_{\rm eq}^{1/2} t^{-2} \tag{4a}$$

for $R < t_{\rm eq}$, and

$$n(R) = \nu R^{-2} t^{-2} \tag{4b}$$

for $R > t_{\rm eq}$. For $R < \gamma\mu G t$

$$n(R) = n(\gamma\mu G t) \tag{5}$$

as can easily be seen by determining the formation time of loops which have radius R at time t.

Loops of size R are not exactly circular. We take this into account by setting the mass of a loop equal to

$$M(R) = \beta\mu R \ . \tag{6}$$

Based on numerical simulations[6,7] $\beta \simeq 9$.

III. ENERGY DENSITY PERTURBATIONS BEFORE RECOMBINATION

The rms energy density fluctuation on a given physical scale k is composed of the contributions from the network of infinite strings and from the distribution of loops. On scales larger than the Hubble radius the contribution from infinite strings dominates; on smaller scales the contribution from loops of radius k^{-1} dominates.

The computation of the contribution from infinite strings is straightforward. The energy density in the infinite string network is

$$\rho(\mathbf{x}) = \sum_i \int ds_i \mu \delta(\mathbf{x} - [\mathbf{d}_i + \mathbf{r}_i(s_i)]) \ , \tag{7}$$

the index i runs over all infinite strings. For each string we choose an origin $\mathbf{d}_i$. $\mathbf{r}_i(s_i)$ is the position a distance s_i along the string measured from $\mathbf{d}_i$ (see Fig. 1). In Fourier space

$$\tilde{\rho}(k) = \sum_i \int ds_i \mu e^{-i\mathbf{k}\cdot\mathbf{d}_i - i\mathbf{k}\cdot\mathbf{r}_i(s_i)} \ . \tag{8}$$

The two-point correlation function of $\tilde{\rho}(\mathbf{k})$ is computed by

averaging over the origin $\mathbf{d}_i$ and the Wiener measure over all paths $\mathbf{r}_i(s_i)$. Since the points $\mathbf{d}_i$ are uncorrelated, terms in $\langle\tilde{\rho}(k)\tilde{\rho}(k')\rangle$ with $i\neq j$ vanish while the diagonal terms $i=j$ give a factor $V^{-1}\delta^3(\mathbf{k}+\mathbf{k}')$, an identical factor for each string. V is a cutoff volume. Hence

$$\langle\tilde{\rho}(\mathbf{k})\tilde{\rho}(\mathbf{k}')\rangle = NV^{-1}\delta^3(\mathbf{k}+\mathbf{k}')\mu^2\int ds\,ds'\langle e^{-i\mathbf{k}\cdot[\mathbf{r}(s)-\mathbf{r}(s')]}\rangle_w \,. \quad (9)$$

N is the total number of paths and $\langle\cdot\rangle_w$ denotes an expectation value under the Wiener measure. For $s'<s$

$$\langle e^{-i\mathbf{k}\cdot[\mathbf{r}(s)-\mathbf{r}(s')]}\rangle_w = Z\int\prod_{s''}dr(s'')\exp\left[-L^{-1}\int r'^2(s'')ds''\right]\exp\left[-i\mathbf{k}\cdot\int_{s'}^{s}ds''\mathbf{r}'(s'')\right]$$
$$= e^{-Lk^2(s-s')/6} \,. \quad (10)$$

$L=L(t)$ is the random-walk correlation length [see Eq. (1)]; Z is the normalization constant. For $s<s'$ the result is identical; s' and s must be interchanged in Eq. (10). The remaining integral over the path parameters s and s' is now trivial. If l is the total length of the string (l is finite in a finite volume V), then

$$\langle\tilde{\rho}(\mathbf{k})\tilde{\rho}(\mathbf{k}')\rangle = 12\frac{Nl}{V}\delta^3(\mathbf{k}+\mathbf{k}')L^{-1}\mu^2k^{-2} \,. \quad (11)$$

$NlV^{-1}\mu$ is the total energy density ρ_s in infinite strings. Hence by Eq. (2)

$$\langle\tilde{\rho}(\mathbf{k})\rho(\mathbf{k}')\rangle = 12\alpha\mu^2k^{-2}L^{-3}\delta^3(\mathbf{k}+\mathbf{k}') \,. \quad (12)$$

The background energy density is

$$\rho_0 = \frac{3}{32\pi}t^{-2}G^{-1} \quad (13)$$

in the radiation-dominated period. In the matter-dominated period the constant prefactor $f=3/32\pi$ is replaced by $f=(6\pi)^{-1}$. Hence

$$\left\langle\frac{\delta\tilde{\rho}}{\rho_0}(\mathbf{k})\frac{\delta\tilde{\rho}}{\rho_0}(\mathbf{k}')\right\rangle = 12\alpha\lambda^{-3}f^{-2}(\mu G)^2k^{-2}t\delta^3(\mathbf{k}+\mathbf{k}') \,. \quad (14)$$

If the power n of k in the two-point correlation function of $\tilde{\rho}(k)$ is in the range $-3<n<4$, then the rms mass excess in a ball of radius $2\pi k^{-1}$ can be immediately determined:[19]

$$\left[\frac{\delta M}{M}\right]^2(k,t) = k^3\delta^{-3}(\mathbf{k}+\mathbf{k}')\left\langle\frac{\delta\rho}{\rho_0}(\mathbf{k})\frac{\delta\rho}{\rho_0}(\mathbf{k}')\right\rangle \,. \quad (15)$$

Combining Eqs. (14) and (15) we obtain

$$\left[\frac{\delta M}{M}\right]^2\Bigg|_{\text{infinite strings}}(k,t) = c(\mu G)^2kt \,, \quad (16)$$

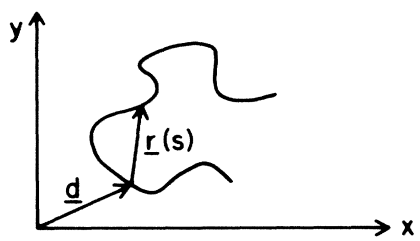

FIG. 1. Parametrization of the random walk.

with $c=12\alpha\lambda^{-3}f^{-2}\sim 4\times10^3$. Note that this is the mean fluctuation due to energy in strings only.

The spectrum of energy density perturbations is scale invariant at Hubble radius crossing, i.e.,

$$\left[\frac{\delta M}{M}\right]^2(k,t_H(k)) = \text{const} \,. \quad (17)$$

[$t_H(k)\sim 2\pi k^{-1}$ is the time when the scale k crosses the Hubble radius.] As has been pointed out before,[3,16,17] this is a consequence of the scale invariance of the network of strings. The power of k ($n=-2$) in Eq. (14) is different from an $n=+1$ Zel'dovich spectrum which arises in many models with linear adiabatic perturbations (e.g., from vacuum fluctuations in the de Sitter phase of inflationary-universe models). The time dependence is different as well. Linear adiabatic perturbations grow faster. $(\delta\rho/\rho)^2$ increases as $t^2(t^{4/3})$ in the radiation-(matter-) dominated phase. The perturbations (14) are compensated on scales larger than the Hubble radius by perturbations of opposite sign in radiation. Thus they, in fact, represent pressure perturbations, which do not grow dynamically in time. The time dependence in Eq. (14) is a kinematic effect.

Next we compute the contribution to the rms mass excess on a given physical scale k by the distribution of loops. For the moment we ignore the spatial correlations of the loops. In Appendix A we show that these correlations are subdominant on scales smaller than the Hubble radius. Typical closed loops oscillate rapidly. We will use a simplified model to compute energy density correlations. We replace a loop of radius R by a spherically symmetric energy density distribution:

$$\rho(r,R) = c(R)e^{-(r/R)^2} \,. \quad (18)$$

$c(R)$ is determined by requiring that the total mass be $\beta\mu R$. The ansatz (18) represents smearing the energy density of the rapidly oscillating loop in time. The resulting energy density correlation function is not sensitive to the details of the smearing. It depends, however, on the exponential cutoff. By the above,

$$c(R) = \pi^{-3/2}\beta\mu R^{-2} \,. \quad (19)$$

The contribution of all loops to the energy density excess is given by

$$\rho(\mathbf{x}) = \sum_i\int d^3\mathbf{r}_i\rho(\mathbf{r}_i,R_i)\delta(\mathbf{x}-(\mathbf{d}_i+\mathbf{r}_i)) \,. \quad (20)$$

$\mathbf{d}_i$ is the position of the center of the loop; $\mathbf{r}_i$ measures the distance from the center. R_i is the radius of loop i. In Fourier space

$$\tilde{\rho}(k)=\sum_i e^{-i\mathbf{k}\cdot\mathbf{d}_i}F(\mathbf{k},R_i) \tag{21}$$

with

$$F(\mathbf{k},R)=c(R)\int d^3\mathbf{r}\, e^{-(r/R)^2}e^{-i\mathbf{k}\cdot\mathbf{r}}$$
$$=\beta\mu R\, e^{-k^2R^2/4}\,. \tag{22}$$

The two-point correlation function is obtained by integrating over the centers $\mathbf{d}_i$ of the loops and by averaging over the radii, using the measure given by the density $n(R)$ of Sec. II:

$$\langle\tilde{\rho}(\mathbf{k})\tilde{\rho}(\mathbf{k}')\rangle=\frac{N}{V}\delta^3(\mathbf{k}+\mathbf{k}')\frac{\int dR\, n(R)F(k,R)^2}{\int dR\, n(R)}\,. \tag{23}$$

The integration domain is $0<R<t$. The denominator in the last factor obviously equals the total number density NV^{-1}. The remaining integral can readily be analyzed by rescaling variables. We define $u\equiv kR$. The numerator in Eq. (23) then becomes

$$\nu\mu^2t^{-3/2}k^{-1/2}\int_{\gamma\mu Gkt}^{kt}du\,u^{-1/2}e^{-u^2/2}$$
$$+\nu\mu^2t^{-4}(\gamma\mu G)^{-5/2}k^{-3}\int_0^{\gamma\mu Gt}du\,u^2e^{-u^2/2}\,. \tag{24}$$

For $\gamma\mu Gtk<1$ the first term dominates and gives

$$c\nu\mu^2t^{-3/2}k^{-1/2} \tag{25a}$$

(c is a constant of order one), while for $\gamma\mu Gkt>1$ the first term is exponentially suppressed. In this case the second term gives

$$\tilde{c}\nu\mu^2(\gamma\mu G)^{-5/2}t^{-4}k^{-3}\,, \tag{25b}$$

where $\tilde{c}$ is another constant of order unity. On scales larger than the Hubble radius expression (23) is independent of k and proportional to t^{-1}. From Eqs. (13) and (15) we conclude that for $t<t_{\rm eq}$

$$\left\langle\frac{\delta\tilde{\rho}(\mathbf{k})}{\rho_0}\frac{\delta\tilde{\rho}(\mathbf{k}')}{\rho_0}\right\rangle=c\nu f^{-2}(\mu G)^2t^{5/2}k^{-1/2}\delta^3(\mathbf{k}+\mathbf{k}'),\quad \gamma\mu Gt<k^{-1}<t\,, \tag{26a}$$

$$\left\langle\frac{\delta\tilde{\rho}(k)}{\rho_0}\frac{\delta\tilde{\rho}(k')}{\rho_0}\right\rangle=\tilde{c}\nu f^{-2}(\mu G)^2(\gamma\mu G)^{-5/2}t^{-4}k^{-3}\delta^3(\mathbf{k}+\mathbf{k}'),\quad k^{-1}<\gamma\mu Gt\,, \tag{26b}$$

and

$$\left[\frac{\delta M}{M}\right]^2(k,t)=c\nu f^{-2}(\mu G)^2(tk)^{5/2},\quad \gamma\mu Gt<k^{-1}<t\,. \tag{27}$$

$\delta M/M$ is constant for $k^{-1}<\gamma\mu Gt$.

For $t>t_{\rm eq}$ the integral in Eq. (23) splits into two terms: the first for $R<t_{\rm eq}$ which looks like Eq. (24) multiplied by $(t_{\rm eq}/t)^{1/2}$, the other for $R>t_{\rm eq}$ which looks like

$$\nu\mu^2t^{-2}k^{-1}\int du\, e^{-u^2/2}\,. \tag{28}$$

The first term dominates for $k^{-1}<t_{\rm eq}$, the second for $k^{-1}>t_{\rm eq}$. Thus for $\gamma\mu Gt_{\rm eq}<k^{-1}<t_{\rm eq}$

$$\left[\frac{\delta M}{M}\right]^2(k,t)=c\nu f^{-2}(\mu G)^2(tk)^{5/2}\left[\frac{t_{\rm eq}}{t}\right]^{1/2} \tag{29}$$

and for $k^{-1}>t_{\rm eq}$

$$\left[\frac{\delta M}{M}\right]^2(k,t)=c\nu f^{-2}(\mu G)^2(tk)^2\,. \tag{30}$$

The spectrum is scale invariant at Hubble radius crossing. The time dependence and k dependence are nonstandard. The time dependence is a purely kinematic effect. At Hubble radius crossing the contributions to the rms mass excess from infinite strings and from finite loops match up to a factor of order 1, as seen from Eqs. (16), (27), and (30). The results are sketched in Fig. 2.

In the absence of cold dark matter no accretion takes place before recombination. Hence the above analysis is valid up to recombination. Cold dark matter starts to accrete around loops at $t_{\rm eq}$. Hence in models with cold dark matter the above analysis holds only for $t<t_{\rm eq}$. We neglect accretion before $t_{\rm eq}$. This can alter the result by a factor of at most $\frac{3}{2}$ (Ref. 19).

Comparison with the results for linear adiabatic perturbations reveals several distinguishing features. There is a distinguished scale below which mass correlations remain constant. Perturbations grow in the radiation-dominated phase even after they enter the Hubble radius. There is no acoustic period. Therefore perturbations on small scales increase by a larger factor than in the case of adiabatic perturbations. Hence at Hubble radius crossing the rms fluctuation can be smaller than in adiabatic linear pertur-

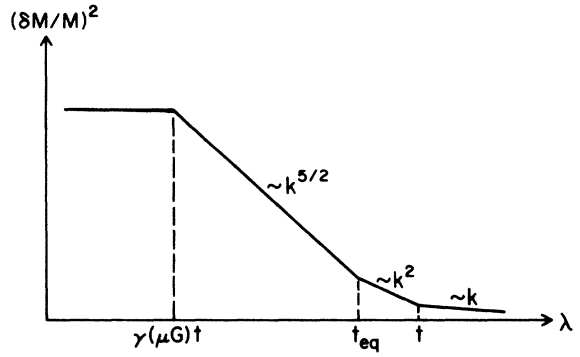

FIG. 2. Energy-density fluctuations before recombination.

bation models without preventing collapse of galaxies and clusters by a red-shift $z \simeq 1$. In fact, using the value $\mu G \sim 2 \times 10^{-6}$ (Ref. 11) we see that $\delta M/M$ is about one order of magnitude smaller. A larger value $\mu G \sim 10^{-5}$ would produce anisotropies in the microwave background greater than present observational upper bounds on large scales (scales corresponding to a distance greater than the Hubble radius at decoupling).

The formation process for cosmic strings conserves energy and momentum. Given an initially homogeneous universe, we must therefore have[20,21]

$$\int d^3\mathbf{x}\, \delta\rho(\mathbf{x}) = 0 , \tag{31a}$$

$$\int d^3\mathbf{x}\, x_k \delta\rho(\mathbf{x}) = 0 . \tag{31b}$$

It then follows that[20,21]

$$\langle \delta\tilde{\rho}(\mathbf{k}) \delta\tilde{\rho}(-\mathbf{k}) \rangle \sim k^4 \tag{32}$$

on large scales. This holds, e.g., for randomly distributed localized perturbations satisfying the above constraints.

$\delta\rho$ in Eqs. (31) and (32) is the total energy density perturbation. It also includes compensating underdensities in radiation. Our calculations only include the contributions from strings. On scales larger than the horizon, Eq. (16) is not relevant for the total energy density perturbation, and hence not for microwave background anisotropies. It is, however, relevant for the correlation function of loops which form from infinite strings. In particular, Eq. (16) is relevant for the correlation function of clusters of galaxies.[22]

On small scales (smaller than the horizon at any time) the underdensities in radiation will spread and damp due to photon diffusion. Hence it makes sense to treat the radiation underdensity as homogeneous and to consider only the density perturbations due to the strings alone.

On large scales, the constraints (31a) and (31b) on the total density perturbation will be satisfied, and thus we do not expect problems with the microwave background radiation anisotropies. We will address this question in more detail in a subsequent publication.[23]

IV. ENERGY DENSITY PERTURBATIONS AFTER RECOMBINATION

Straight, infinite strings do not accrete matter since the local gravitational force vanishes.[24,25] However, closed loops with radius smaller than the Hubble radius do attract matter gravitationally. In the absence of cold dark matter, matter is relativistic before recombination and hence cannot be gravitationally bound. Accretion can start only after recombination. Accretion can be described by the spherical collapse model. In this section we will first summarize the model (for more details see Ref. 19). Then we explain why peculiar velocities of loops can be neglected. Finally, we compute the contribution to the two-point energy density correlation function from collapsed objects, and we determine the complete spectrum of energy density fluctuations.

The spherical model[19] is based on considering a point-like mass m_0 in a universe with critical energy density ($\Omega = 1$). The extra mass will exert a gravitational force on surrounding mass shells. The force will slow down the outward Hubble flow of the mass shells. Eventually, a shell with initial radius r_i will come to rest (in physical coordinates) and start to collapse. According to numerical simulations (see Ref. 1 and references quoted therein), the final radius after collapse will be about $\frac{1}{2}$ of the maximal radius. The equation of motion for a shell of radius r is

$$\frac{1}{2}\dot{r}^2 - \frac{GM}{r} = C , \tag{33}$$

where

$$M = \frac{4\pi}{3}\rho_i r_i^3 + m_0 \tag{34}$$

is the total mass inside the shell. ρ_i is the initial background energy density, r_i the initial radius. The initial velocity $\dot{r}_i$ is given by the Hubble flow $\dot{r}_i = H r_i$, yielding

$$\dot{r}_i^2 = H^2 r_i^2 = \frac{8\pi}{3} G \rho_i \Omega_i^{-1} r_i^2 . \tag{35}$$

C is the total energy. Each loop lies in some background medium of density ρ_i composed of the matter and smaller loops. If this density were critical all shells would eventually collapse. Assume the total energy density in strings plus matter is critical, i.e., $\Omega_{\text{total},i} = 1$. Then each loop lies in a medium of less than critical density. Large radii for which $C > 0$ are unbound and small radii for which $C < 0$ are bound. The radius r_b for which $C = 0$ is given from Eq. (33) by

$$\frac{4\pi}{3}\rho_i r_b^3 (\Omega_i^{-1} - 1) = m_0 . \tag{36}$$

If the density in loops greater than the loop considered is $\epsilon\rho_c$, with ϵ small, then $\Omega_i^{-1} - 1 \simeq \epsilon$, and we see that $r_b \sim d$, where d is the mean separation of loops of the radius considered. Since in any case the spherical model is inappropriate on scales for which competition between loops is important, we conclude that on all relevant scales shells are bound to loops. The case where $\Omega_{\text{total},i} \neq 1$ is more complicated.[11]

For $C < 0$, the solution of Eq. (33) can be written in parametrized form as

$$r = \frac{r_i}{2\Delta_i}(1 - \cos\theta) , \tag{37}$$

$$t = \frac{3t_i}{4\Delta_i^{3/2}}(\theta - \sin\theta) , \tag{38}$$

with

$$\Delta_i = \delta_i - (\Omega_i^{-1} - 1) \simeq \delta_i \tag{39}$$

and

$$\delta_i = \frac{m_0}{\frac{4\pi}{3}\rho_i r_i^3} . \tag{40}$$

A given shell reaches $r_{\max}$ when $\theta = \pi$, at a time

$$t_{\max} = \frac{3\pi}{4}\delta_i^{-3/2} t_i . \tag{41}$$

The spherical collapse model is strictly applicable only for shells always well outside the seed mass. When loops are formed, their average translational velocity is large. According to numerical simulations[7]

$$v_i \sim 0.1 \ . \tag{42}$$

As discussed in Ref. 10, the proper peculiar velocity of a loop

$$v = a\dot{\mathbf{x}} \tag{43}$$

with $\mathbf{x}$ its center of mass in comoving coordinates, redshifts, $v \propto \alpha^{-1}(t)$. The velocity of a loop formed at $t_f < t_{\rm eq}$ with radius $R \sim t_f$ is at $t_{\rm eq}$

$$v_R(t_{\rm eq}) = \frac{a(t_f)}{a(t_{\rm eq})} v_i = \left[\frac{t_f}{t_{\rm eq}}\right]^{1/2} v_i < v_i \tag{44}$$

and the total distance it moves thereafter in comoving coordinates is a fraction $v_R(t_{\rm eq})$ of the horizon scale at $t_{\rm eq}$. For comparison, the mean separation of loops of radius $\sim R$, $d_R(t_{\rm eq})$ is from Eq. (4a)

$$d_R(t_{\rm eq}) = (\tfrac{2}{3}\nu)^{-1/3} R^{1/2} t_{\rm eq}^{1/2} \ . \tag{45}$$

Thus, loops move a fraction

$$\frac{3 v_R t_{\rm eq}}{d_R(t_{\rm eq})} \sim v_i \tag{46}$$

of their mean separation at $t_{\rm eq}$ (using[7] $R \simeq t_f/5$). As long as we consider shells of matter with initial radius $r_i \gg v_i d_R(t_{\rm eq})$ the loop will always be well inside the shell and the spherical collapse model will be valid (this point is not clearly stated in Ref. 10). This is the case for the Abell cluster radius and galaxy radius discussed in Ref. 11, as we show in Appendix B.

Returning to the analysis of the spherical collapse model, we first determine the radius $r_i(t)$ at decoupling of the shell which is beginning to collapse at time t. This radius is obtained by inverting Eq. (41)

$$\delta_i(r_i) = \left[\frac{3\pi}{4}\right]^{2/3} \left[\frac{t_i}{t_{\rm max}}\right]^{2/3} \ . \tag{47}$$

Provided $\delta_i < 1$, the initial radius just collapsing at time t can be determined by inverting Eq. (47)

$$r_i(R,t) \simeq \hat{c} (\mu G)^{1/3} R^{1/3} t_i^{4/9} t^{2/9} \tag{48}$$

with $\hat{c}$ a constant of order one

$$\hat{c} = \left[\frac{9}{2}\right]^{1/3} \left[\frac{4}{3\pi}\right]^{2/9} \beta^{1/3} \ . \tag{49}$$

It only makes sense to apply the spherical collapse model if the initial radius $r_i(R,t)$ beginning to collapse at time t exceeds the loop radius R, i.e., $R < R_c(t)$ where $R_c(t)$ is determined by demanding

$$r_i(R_c,t) = R \tag{50}$$

which gives

$$R_c(t) = \hat{c}^{\,3/2} (\mu G)^{1/2} t_i^{2/3} t^{1/3} \ . \tag{51}$$

At a given time t, for loops with radius R less than $R_c(t)$, the shell which is just collapsing has been outside the loop since t_i.

The energy density distribution around the loop after collapse can be easily determined. If r is the radius and $\rho(r)$ the energy density after collapse, then

$$\rho(r) r^2 dr = \rho_i r_i^2 dr_i \ , \tag{52}$$

r and r_i are related by the spherical model. A shell with initial radius r_i will attain a maximal radius given by Eq. (37)

$$r_{\rm max} = \frac{4\pi}{3\beta} \frac{r_i^4}{\mu R} \rho_i \ . \tag{53}$$

Since $r = \frac{1}{2} r_{\rm max}$, it follows that[19]

$$\rho(r) \simeq \tfrac{1}{3} c^{-3/4} \rho_i^{1/4} (R\mu)^{3/4} r^{-9/4} \ , \tag{54}$$

where

$$c = \frac{2\pi}{3\beta} \ . \tag{55}$$

Equation (54) holds up to the radius which is beginning to collapse at time t, i.e., for $r < r_{\rm max}(R,t)$ where $r_{\rm max}(R,t)$ is related to $r_i(R,t)$ of Eq. (48) by Eq. (53). We obtain

$$r_{\rm max}(R,t) = \hat{\hat{c}} (\mu G)^{1/3} R^{1/3} t_i^{-2/9} t^{8/9}, \quad \hat{\hat{c}} = c \cdot \hat{c}^{\,4} \ . \tag{56}$$

Outside $r_{\rm max}(t)$, the collapse can be described by linear perturbation theory. Since loops which have started to accrete matter can dominate $\delta\rho$ only on small scales, and $\delta\rho$ on small scales samples mainly the core of the energy density perturbations, the precise form of $\delta\rho$ for $r > r_{\rm max}(t)$ is unimportant. We will take $\delta\rho = 0$.

Accretion around loops changes the two-point energy density correlation function. On small scales it is dominated by the peaks of the density distribution, on larger scales it samples the large scale distribution of matter which is unaffected by accretion. We sketch the computation of the correlation function on the various scales in Appendix C. The method is the same as for the loop model in Sec. III.

On the smallest scales ($\lambda < \gamma \mu G t_{\rm dec}$) the spectrum of $\delta M/M$ is flat for the same reason as in Sec. III. For $\gamma \mu G t_{\rm dec} < \lambda < (\mu G)^{1/2} t$ the two-point correlation function reflects the distribution of $\rho(r)$ close to the center of a loop, i.e., Eq. (54). On intermediate scales $(\mu G)^{1/2} t < \lambda < (\mu G)^{1/2} t (t/t_{\rm dec})^{1/2}$ only the total monopole moment of $\rho(r)$ is sampled, and on even larger scales the contribution from loops which have not yet begun to accrete matter dominates, yielding a scaling of $\delta M/M$ as before recombination (Sec. III). On scales larger than the horizon the contribution from infinite strings dominates (see however the discussion of constraints at the end of Sec. III). In Fig. 3 we sketch the result.

Given cold dark matter, accretion starts at $t_{\rm eq}$. The above calculations apply, with $t_{\rm dec}$ replaced by $t_{\rm eq}$ and $\rho_i = \rho(t_{\rm eq})$. In particular, the suppression factor $(t_{\rm eq}/t_{\rm dec})^{1/2}$ in the results (C11), (C12), (C18), and (C19) disappears, reflecting the longer time interval for growth

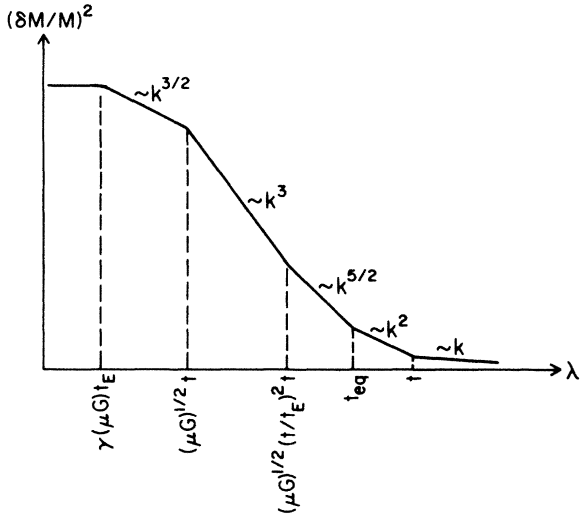

FIG. 3. Energy-density fluctuations after recombination.

of perturbations. The resulting spectrum of energy density perturbations is given by Fig. 3 with $t_{\rm dec}$ replaced by $t_{\rm eq}$. As explained in Ref. 11 the contribution to $\delta M/M$ of wakes which form behind moving strings[10] is subdominant.

V. ANISOTROPIES IN THE MICROWAVE BACKGROUND RADIATION

Inhomogeneities in the early Universe cause anisotropies in the microwave background radiation[12] (MBR). Observations have not yet detected any anisotropies which are not due to the peculiar velocity of Earth, i.e., a dipole term. The best present upper bounds are summarized in Ref. 26. A crucial test of the viability of any cosmological model is that it must not yield too large anisotropies in the microwave background radiation. In a separate publication[11] μG is determined from requirements of galaxy and cluster formation. In this section we show that the predicted anisotropies in the microwave background radiation do not conflict with observations. We first describe the different effects which cause anisotropies; then we discuss the effect of long strings (a Doppler term); finally we give a preliminary quasi-Newtonian analysis of the Sachs-Wolfe[12] effect, the effect of local gravitational perturbations along the light rays.

The temperature T_R of the microwave background radiation today can be expressed in terms of the temperature $T_{\rm dec} \equiv T_E$ at decoupling and the red-shift factor z:

$$\frac{T_R}{T_E} = (1+z_E)^{-1} . \tag{57}$$

The red-shift factor can be rewritten in terms of the wave numbers k_E at decoupling (the last scattering surface) and k_R for the observer. In coordinates in which both source and observer are stationary

$$1+z_E = \frac{k_E}{k_R} . \tag{58}$$

In a more general coordinate system the peculiar velocity of the radiation fluid at $t_{\rm dec}$ and of the observer at the time of observation must be taken into account. Given a peculiar four velocity u we have

$$1+z_E = \frac{(u\cdot k)_E}{(u\cdot k)_R} . \tag{59}$$

The general formula for the variations in the microwave background radiation is[12]

$$\begin{aligned}\frac{\delta T_R}{T_R} &= \frac{\delta T_E}{T_E} + \left[\frac{(\delta u\cdot k)_R}{(u\cdot k)_R} - \frac{(\delta u\cdot k)_E}{(u\cdot k)_E}\right] \\ &\quad + \left[\frac{(u\cdot \delta k)_R}{(u\cdot k)_R} - \frac{(u\cdot \delta k)_E}{(u\cdot k)_E}\right] \\ &= \frac{\delta T_E}{T_E} + \left[\frac{\delta T}{T}\right]_D + \left[\frac{\delta T}{T}\right]_{\rm SW} .\end{aligned} \tag{60}$$

$\delta T_E/T_E$ represents the fluctuations of the last scattering surface; $(\delta T/T)_D$, the term involving δu, is a Doppler term caused by the peculiar velocities of the last scattering surface and of the observer, and the term proportional to δk is the Sachs-Wolfe term due to fluctuations along the light ray.

We assume there are no initial adiabatic perturbations. Perturbations of the last scattering surface and peculiar velocities as last scattering will be considered in Ref. 23. Here we shall consider only the Sachs-Wolfe effect due to loops and a Doppler-type effect on the microwave background, first pointed out by Kaiser and Stebbins.[27] We will start with the latter.

The spacetime around an infinitely long straight string is flat, but has the geometry of R^4 with a wedge $W\times R$ cut out. (See Fig. 4.[24,25]) Consider an observer receiving two light rays from sources passing on opposite sides of the string (Fig. 4). If the string has a velocity $v_\perp$ in the plane normal to the line joining the first source to the observer, the second source will appear to be moving toward

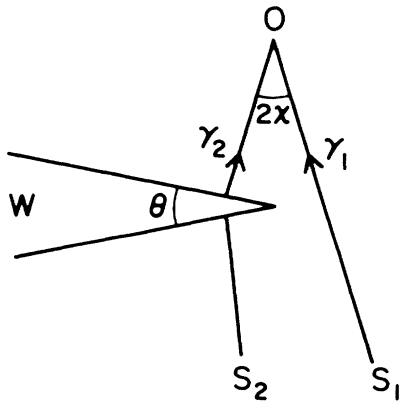

FIG. 4. Gravitational lensing due to cosmic strings. S_1 and S_2 are two light sources; O is the observer; γ_1 and γ_2 are two light rays converging to O.

the observer. The observer will receive the two light rays with a red-shift difference of

$$\Delta\nu = v_\perp \theta = v_\perp 8\pi(\mu G) . \tag{61}$$

A single string would produce a linear discontinuity in the MBR temperature in the sky, but for the value of μG from Ref. 11 and using $v \sim 0.45$ (the average velocity of an oscillating loop segment) it follows that this effect is too small to be observed in present experiments. In the following we also show that the rms fluctuations from this effect due to all strings do not violate the observational bounds on MBR anisotropies.

To compute the rms temperature fluctuation due to long strings on an angular scale θ we must average the contributions of all strings which contribute to the apparent relative velocity of the two light sources (see Fig. 5). The temperature difference is

$$\frac{\delta T}{T}(\theta) = 8\pi(\mu G) \sum_{i=1}^{N} v_\perp . \tag{62}$$

The sum is over all long loops which pierce the wedge of Fig. 5, and long means long compared to the width of the wedge at any time. Since $\langle v_\perp{}^2 \rangle = \frac{2}{3}\langle v^2 \rangle$ and since velocities of two strings are assumed to be uncorrelated, we have

$$\left\langle \frac{\delta T}{T}(\theta)^2 \right\rangle = \frac{128}{3}\pi^2(\mu G)^2 \langle v^2 \rangle N , \tag{63}$$

where $\langle v^2 \rangle$ is the mean-square velocity of a string segment.

The number N of string segments piercing the wedge is

$$\begin{aligned} N &= 2\int_{t_E}^{t_R} dt\, r(t) \mu^{-1} \rho_s(r(t),t) \\ &= 2\int_{t_E}^{t_R} dt\, r(t)\mu^{-1} \int_{r(t)}^{R_{\max}(t)} dR\, \beta R n(R,t) . \end{aligned} \tag{64}$$

$\rho_s(r(t),t)$ is the energy density of loops larger than $r(t)$ at t. $r(t)$ is the half-width of the wedge in Fig. 5 at time t:

$$r(t) = 3t^{2/3}(t_R{}^{1/3} - t^{1/3}) \sin\frac{\theta}{2} . \tag{65}$$

$R_{\max}(t) \sim t$ is the maximal loop radius at time t. For $R(t) < t_{\rm eq}$, formula (4a) for $n(R,t)$ must be used; for $R(t) > t_{\rm eq}$, formula (4b) applies. The integral over radii is dominated by the smallest radii greater than $r(t)$, since their number density is greatest. The time integral is dominated by early times $t \sim t_E$, since the width of the wedge is largest and since the number density decreases in time. Hence on small scales, scales for which $r(t_E) < t_{\rm eq}$, i.e., $\theta < 6' h^{-1}$ (Ref. 19),

$$N = 6\sqrt{3}\beta\nu \left[\sin\frac{\theta}{2}\right]^{1/2} \left[\frac{t_{\rm eq}}{t_E}\right]^{1/2} z(t_E)^{1/4} \tag{66}$$

and on intermediate scales $t_{\rm eq} < r(t_E) < t_E$, i.e., $6' h^{-1} < \theta < 30' \Omega^{1/2}$,

$$N = 18\beta\nu \sin\frac{\theta}{2} z(t_E)^{1/2} . \tag{67}$$

Combining Eqs. (63), (64), and (67) we find ($v = \langle v^2 \rangle^{1/2}$)

$$\left\langle \frac{\delta T}{T}(\theta)^2 \right\rangle^{1/2} = 16\pi 3^{1/4} \beta^{1/2} v \nu^{1/2} \left[\frac{t_{\rm eq}}{t_E}\right]^{1/4} \times z(t_E)^{1/8} \left[\sin\frac{\theta}{2}\right]^{1/4} \mu G \tag{68}$$

on small scales and

$$\left\langle \frac{\delta T}{T}(\theta)^2 \right\rangle^{1/2} = 16\pi 3^{1/2} \beta^{1/2} v \nu^{1/2} z(t_E)^{1/4} \left[\sin\frac{\theta}{2}\right]^{1/2} \mu G \tag{69}$$

on intermediate scales. The transition between the two regions naturally is smooth. With $\mu G \sim 2\times 10^{-6}$ from the accompanying paper (using $\Omega = 1$ and $h = 0.5$) we have

$$\left\langle \frac{\delta T}{T}(\theta)^2 \right\rangle^{1/2} \sim 6\times 10^{-6} \left[\sin\frac{\theta}{2}\right]^{1/4} , \quad \theta < 12' , \tag{70}$$

which gives 6×10^{-6} for $\theta \sim 12'$ and 5×10^{-6} for $\theta \sim 5'$, and is a factor of about 6 smaller than the observational upper bounds.[26] Our small-scale results may be too large. Reionization after recombination will suppress microwave fluctuations on all scales smaller than the horizon at the end of the period of reionization.[28]

Fluctuations from cosmic strings are highly non-Gaussian, so even if the rms value of $\delta T/T$ is below observational limits one could imagine observing local fluctuations. These local fluctuations would be the linelike discontinuities in the microwave background temperature due to a particular string. The magnitude of the discontinuity is $8\pi v \mu G \sim 2\times 10^{-5}$ and thus below observational limits. As pointed out by Kaiser and Stebbins,[27] if the accuracy of the recent measurements by Uson and Wilkinson[29] on angular scales of 5′ could be improved by as little as a factor of 2, such discontinuities could be detected. Since by Eq. (66) the average number strings which would be seen per observation on this angular scale is $\frac{1}{20}$, it would be valuable to measure the anisotropy in many different directions in the sky. The present number (Ref. 29), 12, is marginal.

The second source of anisotropies in the microwave background radiation is the Sachs-Wolfe effect,[12] perturbations in the frequency of the light rays due to local

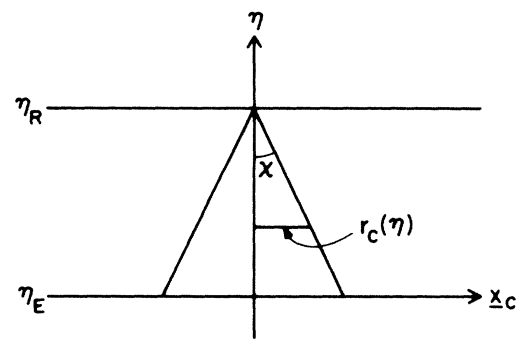

FIG. 5. Conformal space-time diagram of the wedge between two light rays with an angle 2χ.

gravitational perturbations. In our case these are due to finite-size loops.

The general relativistic analysis of this effect is more complicated than for linear adiabatic perturbations. The method is straightforward in principle. Since the frequency four-vector is the tangent vector of the geodesic path of the light ray, the deviation δk_0 of the frequency can be related to the perturbation of the geodesic path, which in turn by the geodesic equation is related to the perturbation of the metric. The difference in k_0 between emission point and observer, the Sachs-Wolfe term in Eq. (60), is thus given by integrating the metric perturbation h_{ij} along the unperturbed light trajectory e:

$$\left[\frac{\delta T}{T}\right]_{\rm SW} = \int_{\eta_E}^{\eta_R} d\eta \tfrac{1}{2} h_{ij,0} e^i e^j \ . \tag{71}$$

h_{ij} is related to the energy density perturbation. It is a good approximation to restrict attention to the growing mode solution in linear perturbation theory, a solution which scales as η^2:

$$h_{ij} = \tfrac{1}{10}\eta^2 A_{,ij}, \quad \frac{\delta\rho}{\rho} = -\tfrac{1}{20}\eta^2 \nabla^2 A \ . \tag{72}$$

In this case, the integral in Eq. (71) may be evaluated explicitly.[12,30] If we subtract the dipole term, the result depends only on $\delta\rho/\rho$ at decoupling.

In models with cosmic strings the energy density correlation functions do not scale in time as η^2. Thus, the analysis immediately becomes technically more difficult. In work in progress[23] we are studying this problem. Here we present a preliminary quasi-Newtonian analysis, which should given the right order of magnitude of the effect.

The Newtonian analysis is based on the following expression[19] for the frequency shift $\delta\nu$ in terms of the Newtonian gravitational potential ϕ:

$$\frac{\delta(a\nu)}{a\nu} = -\int dx^\alpha \frac{\partial\phi(\mathbf{x},t)}{\partial x^\alpha} \ . \tag{73}$$

The line integral is to be taken along the unperturbed light path. The frequency increases while the light ray falls toward the center of the potential and decreases on the way out of the potential well. If the gravitational potential changes in time due to the combined effects of the growth of the density perturbation and the expansion of the Universe, the initial and final potential energies are not the same and light picks up a nontrivial frequency shift while traversing the potential.

In terms of the energy density perturbation $\delta = \delta\rho/\rho$, the Newtonian potential ϕ is given by[19]

$$\phi(\mathbf{x}_c,t) = -G\rho_0 a^2 \int d^3\mathbf{x}' \delta(\mathbf{x}',t) \, | \, \mathbf{x}_c - \mathbf{x}' \, |^{-1} \ . \tag{74}$$

Here x_c denotes comoving coordinates.

We shall evaluate the rms temperature fluctuations due to finite-size loops under the assumption that the light rays pass outside of the support of the energy density perturbation of each loop. The Newtonian potential for each loop can then be developed in a multiple expansion. The monopole term dominates. Hence, the contribution from one loop at $\mathbf{x}=0$ is

$$\phi(\mathbf{x}_c,t) = -G\Delta M(t)\frac{a(t_R)}{a(t)}\frac{1}{|\mathbf{x}_c|} \ . \tag{75}$$

We shall estimate the contribution of one loop to the rms temperature fluctuation on an angular scale χ and average over the position of the loop. The geometry is indicated in Fig. 6. $\mathbf{x}(t)$ and $\mathbf{x}'(t)$ are two light rays converging to the observer with an angle $2\chi=\theta$ between them. The conformal coordinates are

$$\begin{aligned} \mathbf{x}_c(\eta) &= -((\eta_R-\eta)\sin\chi, (\eta_E-\eta)\cos\chi, 0) \ , \\ \mathbf{x}_c'(\eta) &= -((\eta-\eta_R)\sin\chi, (\eta_E-\eta)\cos\chi, 0) \ , \end{aligned} \tag{76}$$

$\mathbf{r}=(x,y,z)$ is the location of the center of the loop in conformal coordinates. $r_x(\eta)$ and $r_{x'}(\eta)$ are the conformal distances between $\mathbf{r}$ and $\mathbf{x}(\eta)$ and $\mathbf{x}'(\eta)$, respectively,

$$\begin{aligned} r_x^2(\eta) &= [x+(\eta_R-\eta)\sin\chi]^2 + [y+(\eta_E-\eta)\cos\chi]^2 + z^2 \ , \\ r_{x'}^2(\eta) &= [x-(\eta_R-\eta)\sin\chi]^2 + [y+(\eta_E-\eta)\cos\chi]^2 + z^2 \ . \end{aligned} \tag{77}$$

Accretion of matter around loops must be taken into account. In the same approximation used in Sec. IV, i.e., $\delta\rho(r)=0$ for $r>r_i$ where r_i is the radius which is just starting to collapse,

$$\Delta M = \beta\mu R + \frac{4\pi}{3}\rho_i r_i^3 \simeq \frac{4\pi}{3}\rho_i r_i^3 \ . \tag{78}$$

For a loop of radius R

$$G\Delta M(R,t) = \frac{2}{g}\hat{c}^3\beta\mu GR\left[\frac{t}{t_E}\right]^{2/3} \ . \tag{79}$$

Hence by Eq. (75)

$$\phi(x_c,t) = \frac{2}{g}\hat{c}^3\beta\mu GR\left[\frac{t_R}{t_E}\right]^{2/3}\frac{R}{|\mathbf{x}_c|} \ . \tag{80}$$

Since the explicit time dependence in ϕ drops out, the line integral in Eq. (73) is trivial (had we neglected accretion, this would not be the case):

$$\frac{\delta\alpha\nu}{a\nu}(\mathbf{x}_c) = \frac{2}{g}\hat{c}^3\beta(\mu G)\left[\frac{t_R}{t_E}\right]^{2/3}\left[\frac{R}{r_x(\eta_R)} - \frac{R}{r_x(\eta_E)}\right] \ . \tag{81}$$

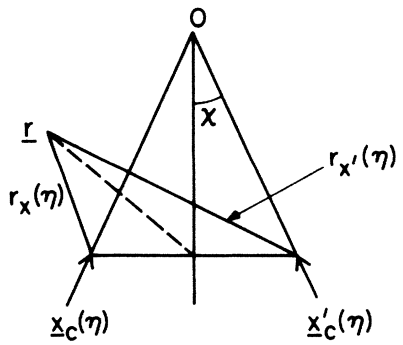

FIG. 6. A loop with center $\mathbf{r}$ contributing to the anisotropy in the microwave background radiation.

Since $r_x(\eta_R)=r_{x'}(\eta R)$

$$\frac{\delta a\nu}{a\nu}(\mathbf{x})-\frac{\delta a\nu}{a\nu}(\mathbf{x}') = \frac{2}{9}\hat{c}^3(\mu G)\left[\frac{t_R}{t_E}\right]^{2/3}\left[\frac{R}{r_{x'}(\eta_E)}-\frac{R}{r_x(\eta_E)}\right]. \quad (82)$$

Loops with radius greater than t_E cannot be described by the formalism. At t_E they still were part of infinite strings. The Sachs-Wolfe effect from infinite strings is shown to be subdominant in Ref. 23.

The rms temperature fluctuation is obtained by averaging the square of the above expression in space and summing over the distribution of radii. Integrating over space we get

$$\int d^3\mathbf{r}\left[\frac{1}{r_{x'}(\eta_E)}-\frac{1}{r_x(\eta_E)}\right]^2 = 8\pi(\eta_R-\eta_E)\sin\chi\ . \quad (83)$$

The number density in comoving coordinates of loops of physical radius R is

$$n_c(R,t_E)=\left[\frac{a(t_E)}{a(t_R)}\right]^3 R^{-5/2}t_E^{-3/2}\nu \quad (84)$$

for $R<t_{\rm eq}$ and

$$n_c(R,t_E)=\left[\frac{a(t_E)}{a(t_R)}\right]^3 R^{-2}t_E^{-2}\nu \quad (85)$$

for $R>t_{\rm eq}$. The integral over R is dominated by the largest loops $R\sim 2t_E$. Hence

$$\left\langle\left[\frac{\delta T}{T}(\mathbf{x})-\frac{\delta T}{T}(\mathbf{x}')\right]^2\right\rangle \simeq \tfrac{48}{9}\pi(\beta\mu G)^2\nu z(t_E)^{1/2}\sin\chi \quad (86)$$

and (using $\chi=\theta/2$)

$$\left\langle\left[\frac{\delta T}{T}(\mathbf{x})-\frac{\delta T}{T}(\mathbf{x}')\right]^2\right\rangle^{1/2} \simeq (48\pi\nu)^{1/2}\tfrac{1}{3}\beta\mu G z(t_E)^{1/4}\sin\frac{\theta^{1/2}}{2}\ . \quad (87)$$

The rms temperature fluctuation is of the order μG. There is no amplitude amplification factor due to accretion, in contrast with the result for the spectrum of energy density fluctuations. Using the values $\mu G\sim 2\times 10^{-6}$, $\nu\sim 10^{-2}$, and $z(t_E)\sim 10^3$ we obtain

$$\left\langle\frac{\delta T}{T}(x)^2\right\rangle^{1/2}\sim 5\times 10^{-5}\sin^{1/2}\frac{\theta}{2},\quad \theta<0.5^\circ\ , \quad (88)$$

which is 2×10^{-6} at $\theta=5'$. We conclude that the Sachs-Wolfe effect and the Kaiser-Stebbins effect both are of the same order of magnitude.

For linear gravitational perturbations[12]

$$\left[\frac{\delta T}{T}\right]^2(\theta)\sim\left[\frac{\delta\rho}{\rho}\right]^2\left[\sin\frac{\theta}{2}\right]^{1-n} \quad (89)$$

given

$$\left[\frac{\delta_\rho}{\rho}\right]^2(k,t_E)=\left[\frac{\delta\rho}{\rho}\right]^2(t_E)k^n\ . \quad (90)$$

By naively applying this prescription to models with cosmic strings, one would obtain roughly the correct amplitude of rms temperature fluctuations [up to the factor $z(t_E)$], but an incorrect angular scaling.

We expect a relativistic analysis to yield a different angular dependence on scales larger than the horizon at decoupling. This will be addressed in a subsequent analysis.[23]

VI. CONCLUSION

We have determined the spectrum of energy density fluctuations and estimated the anisotropies in the microwave background radiation in models with cosmic strings. The analysis is based on a precise mathematical model of the distribution and evolution of strings, a model whose validity has recently been established in numerical simulations. The network of strings consists of a random-walk network of infinite strings with correlation length $L(t)=\lambda t$, and of a scale-invariant distribution of loops which formed between $\gamma\mu Gt$ and t. After recombination, loops accrete baryons; a process described by the spherical collapse model.

The spectrum of energy density fluctuations is constant at Hubble radius crossing (i.e., scale invariant). The dependence on wave number k is not Zel'dovich in the usual sense

$$\frac{\delta M}{M}(k,t)\sim k^2\ . \quad (91)$$

Outside the Hubble radius it scales instead as $k^{1/2}$, inside more steeply (see Figs. 2 and 3).

A quasi-Newtonian analysis is presented which shows that the anisotropies in the microwave background radiation are consistent with the present observational upper bounds, although not much lower. The contributions due to local gravitational perturbations from loops (via the Sachs-Wolfe effect) and due to gravitational lensing by long strings both are of the same order of magnitude.

In future work we intend to give a general relativistic analysis of the anisotropies in the microwave background radiation.[23] We will also discuss higher-order energy density correlation functions as a possible explanation for the existence of voids.[31,32]

ACKNOWLEDGMENTS

For helpful discussions we thank A. Albrecht, T. Kibble, A. Stebbins, J. Traschen, A. Vilenkin, W. Zurek, and in particular J. Deutsch. We also thank A. Vilenkin for carefully reading the manuscript. This research was supported in part by the National Science Foundation under Grant No. PHY82-17853, supplemented by funds from the National Aeronautics and Space Administration, at the University of California at Santa Barbara.

APPENDIX A: EFFECT OF CORRELATIONS BETWEEN LOOPS ON rms QUANTITIES

In the calculation of the spectrum of energy density perturbations and in the determination of the anisotropies of the microwave background radiation we neglected correlations between loops. Here we justify this approximation. We consider the energy density correlation function. The argument is similar for the rms microwave anisotropy.

The Fourier transform of the energy density perturbation from loops is

$$\tilde{\rho}(\mathbf{k}) = \sum_i e^{-i\mathbf{k}\cdot\mathbf{d}_i} F(\mathbf{k},R_i) \ . \tag{A1}$$

The notation is as in Sec. III. In calculating the expectation value of $\tilde{\rho}(\mathbf{k})\tilde{\rho}(\mathbf{k}')$ we must first average over the loop centers $\mathbf{d}_i$. If the loops are correlated, and if $\xi_{R_iR_j}(r)$ denotes the relative overdensity of loops of radii R_i and R_j a distance r apart, then the average is

$$\frac{N}{V}\delta^3(\mathbf{k}+\mathbf{k}')F(\mathbf{k},R)F(-\mathbf{k},R)+\frac{N(N-1)}{V^2}\delta^3(\mathbf{k}+\mathbf{k}')\int d^3\mathbf{r}\, e^{-i\mathbf{k}\cdot\mathbf{r}}\xi_{R_iR_j}(r)F(\mathbf{k},R_i)F(-\mathbf{k},R_j) \ . \tag{A2}$$

The second term contains the effects of loop correlations.

Next, we average over loop radii. Hence

$$\langle\tilde{\rho}(\mathbf{k})\tilde{\rho}(\mathbf{k}')\rangle = \delta^3(\mathbf{k}+\mathbf{k}')\int dR\, n(R)F(\mathbf{k},R)F(-\mathbf{k},R) + \delta^3(\mathbf{k}+\mathbf{k}')\int dR_i dR_j n(R_i)n(R_j)\int d^3\mathbf{r}\, e^{-i\mathbf{k}\cdot\mathbf{r}}\xi_{R_iR_j}(r)F(\mathbf{k},R_i)F(-\mathbf{k},R_j) \ . \tag{A3}$$

The correlation between loops are nonrandom since loops are formed by breaking off from infinite strings, and by splitting of larger loops. According to numerical simulations,[22] the correlation function of loops of similar radius is given by

$$\xi_R(r) = \begin{cases} \epsilon\left[\dfrac{d}{r}\right]^2, & r < d(R) \ , \\ \epsilon\left[\dfrac{d}{r}\right], & r > d(R) \ , \end{cases} \tag{A4}$$

where $d(R)$ is the mean separation of loops larger than R and $\epsilon\sim 0.1$. From Eq. (3), for $t < t_{\rm eq}$, we have

$$d(R) = R^{1/2}t^{1/2}(\tfrac{2}{3}\nu)^{-1/3} \ . \tag{A5}$$

We want to compare the effect of nonrandom centers of loops [the second term in Eq. (A3)] with the result for randomly distributed loops [the first term in Eq. (A3)]. The result for randomly distributed loops is [using Eq. (22)]

$$\int dR\, n(R)F(k,R)^2 = c_1\nu\mu^2 t^{-3/2}k^{-1/2} \tag{A6}$$

with

$$c_1 = \int dx\, x^{-1/2}e^{-x^2/2} \tag{A7}$$

a constant of order one.

In order to evaluate the second term in Eq. (A3) we make the simplifying assumption that only loops of similar radii are nontrivially correlated, i.e.,

$$\xi_{R_iR_j} = R\Delta\delta(R_i - R_j)\xi_{R_i}(r) \tag{A8}$$

with $\xi_{R_i}(r)$ given by Eq. (A4) and $\Delta\sim 1$. By R_k we denote the loop radius for which

$$kd(R_k) = 1 \ . \tag{A9}$$

By Eq. (A5)

$$R_k = t^{-1}k^{-2}(\tfrac{2}{3}\nu)^{2/3} \ . \tag{A10}$$

Now the second term in Eq. (A3), the term which contains the effects of nontrivial correlations, is

$$I(k) = \int dR\, n(R)^2F(k,R)^2R\Delta\int e^{-i\mathbf{k}\cdot\mathbf{r}}\xi_R(r)d^3r = \int dR\, n(R)^2F(k,R)^2R\Delta 4\pi\epsilon \times\left[\frac{d}{k^2}\cos dk+\frac{d^2}{k}\int_0^d dr\, r^{-1}\sin kr\right] . \tag{A11}$$

The first term is the contribution from the large r end of the integration, i.e., from random walk correlations, the second from the small r end, i.e., from correlations between loops which break off larger loops. For $kd < 1$ the first term dominates, for $kd > 1$ the second. Hence

$$I(k) = 4\pi(\tfrac{3}{2})^{1/3}\nu^{5/3}\Delta\epsilon\mu^2k^{-2}(\gamma\mu G)^{-5}t^{1/2}\int_0^{\gamma\mu Gt}dR\, R^{7/2}e^{-k^2R^2/2}+4\pi(\tfrac{3}{2})^{1/3}\nu^{5/3}\Delta\epsilon\mu^2t^{-5/2}k^{-2}\int_{\gamma\mu Gt}^{R_k}dR\, R^{-3/2}e^{-k^2R^2/2} + 2\pi^2(\tfrac{3}{2})^{2/3}\nu^{4/3}\Delta\epsilon\mu^2t^{-2}k^{-1}\int_{R_k}^{\infty}dR\, R^{-1}e^{-k^2R^2/2} \ . \tag{A12}$$

The second term is proportional to $R_{\min}^{-1/2}(t)$ and thus is larger than the third by a factor $\sim(\mu G)^{-1/2}$, at least for scales of the order of the horizon, scales which will be important in the discussion below. The first term, the contribution from loops with $R<\gamma\mu G t$, gives a subdominant effect. On these scales by Eq. (5)

$$I(k)\simeq 8\pi(\tfrac{3}{2})^{1/3}v^{5/3}\Delta\epsilon\mu^2 t^{-3}k^{-2}\gamma^{-1/2}(\mu G)^{-1/2} . \quad \text{(A13)}$$

The ratio between Eqs. (A13) and (A6) is

$$8\pi(\tfrac{3}{2})^{1/3}\gamma^{-1/2}c_1^{-1}\Delta\epsilon(\mu G)^{-1/2}v^{2/3}(tk)^{-3/2} \sim 30\frac{\Delta}{c_1}(tk)^{-3/2} . \quad \text{(A14)}$$

As a consistency check, we note that the ratio between the third term in Eq. (A12) and (A6) is suppressed for $tk>1$ by $(tk)^{-1/2}$.

We conclude that on scales smaller than the Hubble radius, loop correlations are unimportant. Outside the Hubble radius, however, they begin to dominate the root-mean-square energy density fluctuations. The main contribution is due to the random-walk correlations of loops at large distances.

APPENDIX B: PECULIAR VELOCITIES OF LOOPS

Peculiar velocities of loop are negligible for galaxy and Abell cluster formation considerations. The physical distance Δx loops around which galaxies and Abell clusters accrete travel between $t_{\rm eq}$ and the present time t is smaller than the initial radius r_i at $t_{\rm eq}$ of the shells which collapse to a galactic or Abell cluster radius. We now demonstrate this result.

A loop which was formed at time t_f with velocity v_i travels a physical distance

$$\Delta x_p(t)=3v_i\left[\frac{t_f}{t_{\rm eq}}\right]^{1/2}\left[\frac{t}{t_{\rm eq}}\right]^{2/3}t_{\rm eq} \quad \text{(B1)}$$

between $t_{\rm eq}$ and t. The corresponding physical distance at $t_{\rm eq}$ is

$$\Delta x_p(t_{\rm eq})=3v_i\left[\frac{t_f}{t_{\rm eq}}\right]^{1/2}t_{\rm eq} . \quad \text{(B2)}$$

According to numerical simulations,[7] primary loops with radius of the order of the horizon distance are formed by intersections of infinite strings, and then break up into on the average p secondary loops of radius R where[7] $p\sim 10$. Hence, on the average,

$$t_f=\left[\frac{p}{2}\right]R . \quad \text{(B3)}$$

On the other hand, the initial proper radius of a shell which collapses at a red-shift $1+z_{\max}$ to a final virialized radius r is given by Eqs. (37) and (41):

$$r_i=\left[\frac{3\pi}{4}\right]^{2/3}2\frac{1+z_{\max}}{1+z_{\rm eq}}r = \left[\frac{3\pi}{4}\right]^{2/3}\frac{2r}{t}(1+z_{\max})(1+z_{\rm eq})^{1/2}t_{\rm eq} . \quad \text{(B4)}$$

We now compare Eqs. (B2) and (B4) for a shell of Abell cluster radius. From Ref. 11 $1+z_{\max}\simeq 1.6$, $r\simeq 1.5h^{-1}$ Mpc, and

$$\left[\frac{R}{t_{\rm eq}}\right]=0.67(\Omega h)^2 . \quad \text{(B5)}$$

With $p=10$, $v_i=10^{-1}$, and $t=2\times 10^3 h^{-1}$ Mpc we get

$$\Delta x_p(t_{\rm eq})\simeq 5\times 10^{-1}\Omega h t_{\rm eq} \quad \text{(B6)}$$

and

$$r_i\simeq 7\times 10^{-1}\Omega^{1/2}h t_{\rm eq} . \quad \text{(B7)}$$

Thus the spherical collapse model is valid when considering the accretion of Abell clusters. Comparing (B5) with (B7) we see that this shell was always outside the loop radius.

For a shell which virialized at a galactic radius $r\simeq 20h^{-1}$ kpc we use[11] $1+z_{\max}\simeq 10$ and

$$\frac{R}{t_{\rm eq}}=5.5\times 10^{-3}(\Omega h)^2 . \quad \text{(B8)}$$

Hence with $p=10$ and $v_i=10^{-1}$

$$\Delta x_p(t_{\rm eq})\simeq 5\times 10^{-2}\Omega h t_{\rm eq} \quad \text{(B9)}$$

and

$$r_i\simeq(1+z_{\max})6\times 10^{-3}h\Omega^{1/2}t_{\rm eq} \simeq 6\times 10^{-2}h\Omega^{1/2}t_{\rm eq} . \quad \text{(B10)}$$

r_i exceeds $\Delta x_p(t_{\rm eq})$ and hence peculiar velocities are negligible. Comparing (B8) with (B10) we see that the shell was always outside the loop radius.

APPENDIX C: COMPUTATION OF THE TWO-POINT CORRELATION FUNCTION AFTER RECOMBINATION

The computation of the two-point energy density correlation function is similar to the calculation in the loop model of Sec. III. The energy density perturbation is given by Eqs. (20) and (21), using $\rho(R,r)$ from Eq. (54) with $\rho_i=\rho(t_{\rm dec})$ and $t_i=t_{\rm dec}$:

$$\tilde{\rho}(\mathbf{k})=\sum_j e^{-i\mathbf{k}\cdot\mathbf{d}_j}F(k,R_j) \quad \text{(C1)}$$

with

$$F(k,R)=\int d^3\mathbf{r}\,\rho(R,r)e^{-i\mathbf{k}\cdot\mathbf{r}} =\frac{4\pi}{3}c^{-3/4}\rho_i^{1/4}(R\mu)^{3/4}k^{-1} \times\int_0^{r_{\max}(R,t)}dr\,r^{-5/4}\sin kr . \quad \text{(C2)}$$

On large scales, i.e., $kr_{\max}<1$,

$$F(k,R)\simeq\frac{16\pi}{9}c^{-3/4}\rho_i^{1/4}(R\mu)^{3/4}r_{\max}(R,t)^{3/4}\ . \quad \text{(C3)}$$

On small scales with $x=kr$

$$F(k,R)\simeq\frac{4\pi}{3}c^{-3/4}\rho_i^{1/4}(R\mu)^{3/4}k^{-3/4}\times\int_0^{kr_{\max}}dx\,x^{-5/4}\sin x\ . \quad \text{(C4)}$$

Since the integral is dominated by $x<1$, it can be replaced by a constant $\tilde{c}$. Thus on small scales

$$F(k,R)=\frac{4\pi}{3}\tilde{c}c^{-3/4}\rho_i^{1/4}(R\mu k^{-1})^{3/4}\ . \quad \text{(C5)}$$

The two-point energy density correlation function from loops which have started to accrete matter by the time t is obtained by averaging over the centers $\mathbf{d}_i$ and over the number density $n(R)$:

$$\langle\tilde{\rho}(\mathbf{k})\tilde{\rho}(\mathbf{k}')\rangle=\delta^3(\mathbf{k}+\mathbf{k}')\int_{R_{\min}(t)}^{R_c(t)}dR\,n(R)F(k,R)^2\ . \quad \text{(C6)}$$

Using Eq. (51) and the value $\mu G\sim10^{-6}$ it follows that $R_c(t)$ is smaller than $t_{\rm eq}$ for all times. Hence $n(R)$ is given by Eq. (4a).

For given t and k we define $R_c(t,k)$ as the radius R for which

$$r_{\max}(R_c(t,k),t)k=1\ . \quad \text{(C7)}$$

If $R<R_c(t,k)$, then expression (C3) for $F(k,R)$ must be used in the above integral; if $R>R_c(t,k)$ then Eq. (C5) holds. From Eq. (56) it follows that

$$R_c(t,k)=\hat{\hat{c}}^{-3}(\mu G)^{-1}t_i^{2/3}t^{-8/3}k^{-3}\ . \quad \text{(C8)}$$

On intermediate scales $R_c(t)<R_c(t,k)$. Hence expression (C3) can be used for all R. The result is

$$\langle\tilde{\rho}(\mathbf{k})\tilde{\rho}(\mathbf{k}')\rangle=\delta^3(\mathbf{k}+\mathbf{k}')c_1(\mu G)^{3/4}\mu^{3/2}\rho_i^{1/2}\left[\frac{t_{\rm eq}}{t}\right]^{1/2} \quad \text{(C9)}$$

with

$$c_1=2\nu\left[\frac{16\pi}{9}\right]^2c^{-3/2}\hat{c}^{3/4}\hat{\hat{c}}^{3/2}\ . \quad \text{(C10)}$$

Hence

$$\left\langle\frac{\delta\tilde{\rho}}{\rho_0}(\mathbf{k})\frac{\delta\tilde{\rho}}{\rho_0}(\mathbf{k}')\right\rangle=\delta^3(\mathbf{k}+\mathbf{k}')c_1(6\pi)^{3/2}(\mu G)^2(\mu G)^{1/4}t_{\rm dec}^{\,3}\times\left[\frac{t}{t_{\rm dec}}\right]^{7/2}\left[\frac{t_{\rm eq}}{t_{\rm dec}}\right]^{1/2} \quad \text{(C11)}$$

and by Eq. (15)

$$\left[\frac{\delta M}{M}\right]^2(k,t)=c_1(6\pi)^{3/2}(\mu G)^2(\mu G)^{1/4}(kt)^3\times\left[\frac{t}{t_{\rm dec}}\right]^{1/2}\left[\frac{t_{\rm eq}}{t_{\rm dec}}\right]^{1/2}\ . \quad \text{(C12)}$$

From Eq. (C11) it follows that loops which have accreted matter around them on large scales induce energy density fluctuations with the same k dependence as is obtained for a random distribution of localized blobs of matter. The loop nature of the perturbations is hidden on intermediate scales.

On small scales the integral in Eq. (C6) splits into two terms:

$$\int_{R_{\min}(t)}^{R_c(t)}dR\,n(R)F(k,R)^2=\int_{R_{\min}(t)}^{R_c(t,k)}dR\,n(R)F(k,R)^2+\int_{R_c(t,k)}^{R_c(t)}dR\,n(R)F(k,R)^2\ . \quad \text{(C13)}$$

By Eqs. (C3), (56), and (51), the first term becomes

$$c_2\rho_i^{1/2}\mu^{3/2}t_{\rm eq}^{1/2}t^{-2}k^{-3/2} \quad \text{(C14)}$$

and by Eq. (C5) the second term is

$$c_3\rho_i^{1/2}\mu^{3/2}t_{\rm eq}^{1/2}t^{-2}k^{-3/2}\ln\frac{R_c(t)}{R_c(t,k)}\ , \quad \text{(C15)}$$

with

$$c_2=2\nu\left[\frac{16\pi}{9}\right]^2c^{-3/2} \quad \text{(C16)}$$

and

$$c_3=\nu'\left[\frac{4\pi}{4}\right]^2\hat{c}^2c^{-3/2}\ . \quad \text{(C17)}$$

Both terms have the same k dependence and the same amplitude, but the second dominates by the logarithmic factor. Thus

$$\left\langle\frac{\delta\tilde{\rho}}{\rho_0}(\mathbf{k})\frac{\delta\tilde{\rho}}{\rho_0}(\mathbf{k}')\right\rangle=\delta^3(\mathbf{k}+\mathbf{k}')c_3(6\pi)^{3/2}(\mu G)^{3/2}\left[\frac{t}{t_{\rm dec}}\right]^{1/2}\left[\frac{t_{\rm eq}}{t_{\rm dec}}\right]^{1/2}\times(tk^{-1})^{3/2}\ln\frac{R_c(t)}{R_c(t,k)} \quad \text{(C18)}$$

and

$$\left[\frac{\delta M}{M}\right]^2(k,t)=c_3(6\pi)^{3/2}(\mu G)^{3/2}(tk)^{3/2}\times\left[\frac{t}{t_{\rm dec}}\right]^{1/2}\left[\frac{t_{\rm eq}}{t_{\rm dec}}\right]^{1/2}\ln\frac{R_c(t)}{R_c(t,k)}\ . \quad \text{(C19)}$$

On small scales the energy density correlation function

for loops differs from that for randomly distributed point perturbations. The expressions (C12) and (C19) match up to factors of order 1 at the scale on which $R_c(t)=R_c(t,k)$. This scale is given by

$$kt \sim (\mu G)^{-1/2} . \tag{C20}$$

In Fig. 3 we sketch the rms mass fluctuations after recombination. For very small scales Eq. (C19) dominates, for intermediate scales the loops which have accreted matter still dominate the mass fluctuations, but have a spectrum as expected for randomly distributed point perturbations, and for scales larger than k_c^{-1} the fluctuations from large loops which have not yet accreted matter form the largest contribution. By comparing Eqs. (29) and (C12) we find

$$k_c t \sim (\mu G)^{-1/2} \left[\frac{t_{\rm dec}}{t} \right] . \tag{C21}$$

Finally, on scales larger than the Hubble radius the network of infinite strings gives the most important term.

---

*Present address: DAMTP, University of Cambridge, Silver Street, Cambridge, CB3 9EW, United Kingdom.

†Present address: Department of Theoretical Physics, Imperial College, London SW7, United Kingdom.

[1]J. Primack, SLAC-PUB-3387, lectures presented at the International School of Physics "Enrico Fermi," Varenna, Italy, 1984 (unpublished).

[2]Ya. Zel'dovich, Mon. Not. R. Astron. Soc. **192**, 663 (1980).

[3]A. Vilenkin, Phys. Rev. Lett. **46**, 1169 (1981); **46**, 1496(E) (1981); A. Vilenkin, Phys. Rev. D **24**, 2082 (1981).

[4]T. W. B. Kibble, J. Phys. A **9**, 1387 (1976); Phys. Rep. **67**, 183 (1980).

[5]A. Vilenkin, Phys. Rep. **121**, 263 (1985); T. W. B. Kibble, in *Quantum Structure of Spacetime,* edited by M. J. Duff and C. J. Isham (Cambridge University Press, Cambridge, 1982).

[6]A. Albrecht and N. Turok, Phys. Rev. Lett. **54**, 1868 (1985).

[7]A. Albrecht and N. Turok (unpublished).

[8]N. Turok, Phys. Lett. **123B**, 387 (1983).

[9]A. Vilenkin and Q. Shafi, Phys. Rev. Lett. **51**, 1716 (1983).

[10]J. Silk and A. Vilenkin, Phys. Rev. Lett. **53**, 1700 (1984).

[11]N. Turok and R. Brandenberger, Phys. Rev. D **33**, 2175 (1986).

[12]R. Sachs and A. Wolfe, Astrophys. J. **147**, 73 (1967).

[13]T. Vachaspati and A. Vilenkin, Phys. Rev. D **30**, 2036 (1984).

[14]R. Scherrer and J. Frieman, Phys. Rev. D (to be published).

[15]N. Turok and P. Bhattacharjee, Phys. Rev. D **29**, 1557 (1984).

[16]T. W. B. Kibble, Nucl. Phys. **B252**, 277 (1985).

[17]N. Turok, Nucl. Phys. **B242**, 520 (1984).

[18]T. Vachaspati and A. Vilenkin, Phys. Rev. D **31**, 3052 (1985).

[19]P. J. E. Peebles, *The Large Scale Structure of the Universe* (Princeton University Press, Princeton, New Jersey 1980).

[20]Ya. Zel'dovich, Adv. Astron. Astrophys. **3**, 241 (1965).

[21]J. Traschen, Phys. Rev. D **29**, 1563 (1984).

[22]N. Turok, Phys. Rev. Lett. **55**, 1801 (1985).

[23]J. Traschen, N. Turok and R. Brandenberger, ITP Report No. NSF-ITP-85-110, 1985 (unpublished).

[24]A. Vilenkin, Phys. Rev. D **23**, 852 (1981).

[25]D. Garfinkle, Phys. Rev. D **32**, 1323 (1985).

[26]D. Wilkinson, in *Proceedings of the Inner Space/Outer Space Conference, Fermilab* edited by E. Kolb, M. S. Turner, D. Lindley, K. Olive, and D. Seckel (University of Chicago, Chicago, 1985).

[27]N. Kaiser and A. Stebbins, Nature (London) **310**, 391 (1984).

[28]C. Hogan, N. Kaiser and M. Rees, Philos. Trans. R. Soc. London **A307**, 97 (1982).

[29]J. Uson and D. Wilkinson, Astrophys. J. **277**, L1 (1984).

[30]J. Traschen, Ph.D. thesis, Harvard University, 1984.

[31]N. Turok and D. Schramm, Nature (London) **312**, 598 (1984).

[32]A. Albrecht, R. Brandenberger, and N. Turok, ITP Report No. NSF-ITP-85-96, 1985 (unpublished).